Defect Diagnosis of Distributed Power Cable Terminal Based on Electromagnetic Coupling Characteristics

Lappeenranta–Lahti University of Technology

LUT Bachelor’s Programme in Electrical Engineering,

Bachelor's thesis

2026

Ruidong Wang

Examiner(s): Professor Yunqi Xing

Hafiz Majid Hussain, D.Sc. (Tech.)

ABSTRACT

Lappeenranta–Lahti University of Technology LUT

Your school: LUT School of Engineering Sciences

Your degree programme: Electrical Engineering

In co-operation with partner university: Hebei University of Technology

Ruidong Wang

Defect Diagnosis of Distributed Power Cable Terminal Based on Electromagnetic Coupling Characteristics

Bachelor's thesis

2026

38 pages, 17 figures, 3 tables

Examiner(s): Professor Xing Yunqi and Hafiz Majid Hussain, Ph.D.

Keywords: XLPE cable termination; Typical defects; Electromagnetic field simulation; Statistical characteristics; Defect identification

At present, the defect of the cable terminations is caused by the manual installation. Such defects cause local distortion of the electric field and cause degradation of the insulation, so the research of the types of faults in the cable is an important problem that needs to be studied. This paper takes 35 kV cross-linked polyethylene (XLPE) cable terminations as the research object and conducts simulation and intelligent identification studies on the transient electromagnetic response of typical defects. Based on the structural parameters of an actual Raychem 35 kV three-core medium-voltage cable termination model, a three-dimensional model was established using SolidWorks modeling software, and three insulation damage models were established: main insulation scratches, air gaps, and metal particles. Transient electromagnetic wave simulation analysis was performed using COMSOL simulation software. The results show that among the three typical defects, metal particle defects produce the highest peak electric field intensity (5200 V/m), followed by air gap defects (315 V/m), and scratch defects (135 V/m) produce the lowest. Regarding waveform characteristics, the observation point measurement results show significant differences in pulse width, oscillation number, dominant frequency, and attenuation characteristics. Among them, metal particle defects have the richest high-frequency components, with a dominant frequency of approximately 3.0 GHz. Features were extracted and a support vector machine (SVM) model was used to analyze the defect types. Using five-fold cross-validation, the overall classification accuracy of various defects reached

99.67%. Among them, the recognition rate of scratch defects was 100%, and the recognition rates of air gap defects and metal particle defects both reached 99.5%. This paper establishes an intelligent classification method based on defect geometry and electromagnetic propagation characteristics, providing theoretical support for online monitoring and condition assessment of cable terminals.

SYMBOLS AND ABBREVIATIONS

Roman characters

D	Electric flux density	C/m²
E	Electric field intensity	V/m
V	Electric potential	V
$V0$	Peak amplitude of Gaussian pulse	kV
$t0$	Pulse centre time	ns
t	Time	s
tw	Pulse width	ns
W	Signal energy	J
fd	Dominant frequency	GHz
$Nosc$	Number of oscillations	
x	Feature vector	
C	Penalty parameter in SVM	
K	Kernel function	
f	Frequency	Hz

Greek characters

$\varepsilon 0$	Vacuum permittivity	F/m
εr	Relative permittivity	
ρv	Space charge density	C/m³
σ	Electrical conductivity	S/m
τ	Pulse width parameter	ns
η	Attenuation ratio	
μ	Mean value	
γ	Kernel coefficient in RBF function	

Abbreviations

XLPE	Cross-linked polyethylene

PD	Partial discharge
UHF	Ultra-high frequency
HFCT	High-frequency current transformer
FFT	Fast Fourier Transform
SVM	Support Vector Machine
ECOC	Error Correcting Output Codes
RBF	Radial Basis Function
ANN	Artificial Neural Network
CNN	Convolutional Neural Network
GIS	Gas Insulated Switchgear

Table of contents

1. Introduction 1
1.1 Research Background 1
1.2 Current Status of Research on Cable Terminal Defect Detection 2
1.3 This thesis studies the content of the research. 4
2. Modelling of 35 kV XLPE cable termination structure and defects 6
2.1. 3D geometric modelling of cable terminals 6
2.1.2. Simulation parameters and boundary conditions 8
2.1.3. Physics field selection and boundary conditions 9
3. Comparative Analysis of Transient Electromagnetic Responses under Different Defect Types 11
3.1 Main insulation scratch defects 11
3.2 Air gap defects 14
3.3 Metal particle defects 16
4. Signal Propagation Characteristics Extraction and Mathematical Analysis under Typical Defect Conditions 19
4.1 Time-Domain Feature Extraction 19
4.2 Frequency-Domain Characteristic Analysis 19
4.3 Quantitative Comparison of Different Defects 20
4.4 Defect Classification Based on Support Vector Machine 20
4.5 Model accuracy analysis and result evaluation 21
5. Conclusions 25
5.1 Future Work Outlook 26
References 29

Figures

Figure 1. Schematic diagram of cable terminal stripping

Figure 2. Cable terminal cross-section

Figure 3. Low-voltage end structure and details

Figure 4. Main insulation scratch defects

Figure 5. Air gap defects

Figure 6. Metal particle defects

Figure 7. Mesh partitioning diagram

Figure 8. Electric field distribution at the scratch at 81 mm

Figure 9. Scratch observation point

Figure 10. Bottom low-pressure end observation point under scratch defect

Figure 11. Electric field diagram of an air gap defect with a diameter of 1 mm

Figure 12. Air gap observation point

Figure 13. Bottom low-pressure end observation point under air gap defect

Figure 14. Electric field diagram of metal particle defects

Figure 15. Metal particle observation point

Figure 16. Bottom low-pressure end observation point under metal particle defect

Figure 17. Confusion Matrix of SVM-Based Cable Terminal Defect Classification

Tables

Table 1. Cable termination structure and material properties table

Table 2. Eigenvalue table of different defect characteristics

Table 3. Precision and recall rates for each defect category

DECLARATIONS

Turnitin

The originality of this thesis has been reviewed with the Turnitin similarity checking service.

AI usage

The author of the thesis, Ruidong. Wang, used the following AI-tools during the preparation of the thesis:

1. Grammarly
    a. Purpose of use: To ensure sentences are expressed correctly and accurately.
    b. Explanation of the use of the tool: This tool is used to optimize the grammar, sentence structure, and accuracy of the paper. All revisions are reviewed by the author.

The author, Ruidong. Wang, takes full responsibility for the content of this thesis and has reviewed and edited the content generated by the possible use of AI tools.

1. Introduction

1.1 Research Background

In China, 35kV transmission cables are widely used in urban power distribution networks, industrial parks, and other production and daily life sectors. Due to their commonality and importance, they have become a common subject of domestic research. Cross-linked polyethylene (XLPE) cables are the mainstream cable type, possessing excellent thermal, mechanical, and electrical properties, as well as advantages such as simple cable structure and ease of installation and maintenance (Tanaka, 2005). 35kV cable terminals are high-risk areas for cable faults; statistical analysis over many years has revealed that internal insulation defects in the terminals account for more than 50% of all accidents (Liu & Chen, 2012). Due to structural complexity and installation factors, cable accessories (including terminals and joints) are more prone to insulation degradation than the cable itself (Morshuis, 2005). The fabrication and installation of cable terminals mainly rely on manual labour. Factors such as the technical level of construction personnel, the implementation of process specifications, and on-site environmental conditions may increase the risk of defects to a certain extent.

Common cable terminal defects include: (1) scratches on the main insulation caused by failure to control the ring stripping depth; (2) air gap defects caused by manufacturing process or environment; (3) metal particle defects, etc. It can create uneven electric field distribution due to irregular edges and corners. Such activities can cause electrical sparks to occur in these places over time, which can eventually cause insulation failure (Li Ming et al., 2004).

It is therefore very desirable to accurately detect the type and location of fault points during normal cable operation and maintenance to detect and identify the hazard at an early stage, estimate the cable service life and formulate the maintenance plan.

The use of technology for cable condition monitoring by spark discharge (PD) detection has been widely taken-up in recent years. It helps to evaluate the insulation condition of cables and the detection of fault condition in an early stage (Shafiq et al., 2019).

Electromagnetic signal analysis has been a topic of great interest as a means of monitoring. This is because they are the pulses produced by electrical discharges that are able to pass through the cable structure and be detected remotely, making the process of diagnostics possible without touching the cable (Kaziz et al., 2023).

1.2 Current Status of Research on Cable Terminal Defect Detection

The studies of the defect of the cable terminal in China mainly focus on the electric field simulation, properties of partial discharge and optimization technique of the structure of the terminal. From the vantage point of defect mechanisms and electric field distribution patterns, Liu Gang's research team at South China University of Technology conducted an inquiry into air-gap defects in 2012, employing power-frequency electrostatic field analysis. Their findings revealed that a reduced air gap within the primary insulation of cable terminals precipitates more pronounced electric field distortion. They also pointed out that the OWTS testing system can effectively detect air-related defects at the main insulation of cable terminals (Li, 2022). Li Haomeng et al. at Harbin University of Science and Technology found that after thermal aging, the conductivity of XLPE and silicone rubber materials mainly decreases with increasing aging time, while the relative permittivity increases in the opposite direction. They derived a conductivity formula for silicone rubber materials with electric field strength and temperature as variables. When the root angle between the main insulation and the reinforcing insulation of the cable satisfies $\alpha = 27°\sim31°$, the cable terminal meets the optimal design for electric field distribution (Li, 2022) The existence of edge shield tip and conductive impurities is more likely to induce strong discharge (Huang, 2022). Yanghongquan, a researcher from Chengdu power supply company, and other researchers have successfully detected and accurately located the partial discharge defects in GIS cable terminals by using ultra-high frequency (UHF) and high frequency current transformer (HFCT) methods and technical means. After completing the theoretical test, the accuracy of the positioning results was further verified by removing the cable (Hongquan et al., 2022). In general, the domestic research mainly focuses on power frequency electric field simulation, partial discharge experiment and stress cone structure optimization. However, most of the current studies only focus on the analysis of steady-state electric field and the

comparison of experimental partial discharge waveforms. The research on the transient electromagnetic coupling characteristics under ultrafast excitation is still relatively limited and scarce. International scholars have carried out extensive and in-depth research on insulation degradation mechanism and electromagnetic behavior. Canadian researchers, including hazleeazil illias, have found that defects such as air gap, delamination and cusp can lead to serious concentration of local electric field, which is easy to induce partial discharge. Improving the dielectric constant of the insulating material helps to reduce the electric field strength at the defect, thereby improving the operation reliability of the cable joint (Illias et al., 2012). In the field of diagnosis methods, Govindarajan et al. (2023) proposed that partial discharge (PD) diagnosis of power cables includes three stages: detection, location and classification, and pointed out that partial discharge location plays an important role in evaluating the degree of insulation defects and formulating maintenance strategies. This review also systematically summarizes the research progress and limitations of existing technologies in automatic recognition of different partial discharge characteristics (Govindarajan et al., 2023). At the same time, the partial discharge modelling theory has also been deeply and systematically studied. Niemeyer proposed a generalized partial discharge model, which established the relationship between defect characteristics and measurable discharge parameters, and laid a theoretical foundation for the modelling of equivalent partial discharge power supply (Niemeyer, 1995). A team led by Japanese scholar Yoshiya Yamashita has developed a partial discharge locator (PDL), which can locate partial discharge by measuring the time difference of current pulse signal. Through the application of GPS and other synchronous acquisition technologies, the research results show that the defect location can be determined relatively accurately (Yamashita et al., 2019).

In the field of electromagnetic signal detection, Donald M. Hepburn and Bojie Sheng in the UK have found that partial discharge pulses generated by insulation defects can propagate along cables in the form of electromagnetic waves and can be detected over long distances, which provides a basis for electromagnetic-based diagnostic methods (Sheng et al., 2014).

Overall, existing research on cable terminal defect diagnosis from China and abroad can be roughly divided into three research directions: electric field simulation analysis, partial discharge detection technology and intelligent diagnostic algorithms. Electric field simulation research mainly focuses on analysing static or power frequency electric field distortions caused by defects, revealing the mechanisms of local electric field enhancement

under different defect geometries. In terms of detection technology, partial discharge detection remains the mainstream method, including pulsed current methods, high-frequency current transformers (HFCTs), ultra-high frequency (UHF) detection, acoustic emission, and optical methods. Meanwhile, with the development of artificial intelligence technology, machine learning algorithms such as support vector machines (SVMs), neural networks, and random forests have been widely applied to the classification and identification of partial discharge modes, significantly improving the level of automated diagnosis.

Despite significant progress in experimental studies in recent years, certain limitations remain. Most simulation studies are based on quasi-static field research, such as studying field strength in defect states, with insufficient attention paid to transient electromagnetic propagation characteristics caused by rapid discharge excitation. Furthermore, there is a lack of systematic modelling that links defect geometry, material properties, and signal spectral characteristics; the relationship between observable transient electromagnetic waveforms and physical field distributions is not fully elucidated. Furthermore, there has been no mature and reliable mathematical model for the intelligent diagnosis of cable defects based on electromagnetic field, and there is no unified quantitative feature mapping mechanism. Partial discharge diagnostic techniques are still used, but have many drawbacks including noise interference, multiple source separation, and poor remaining life estimation capabilities (Stone, 2005). Based on these shortcomings, further research is encouraged on the coupling linearity between electromagnetic propagation characteristics of cable defect and signal propagation laws, which can be used to aid the defect identification and online detection in production.

1.3 This thesis studies the content of the research.

Based on existing research and actual 35kV cable terminal parameters, the main contents of this study are as follows:

1) Modelling and Simulation of Defective Cable Terminations

As per the structural characteristic of 35 kV cable terminal, the paper proposes a three dimensional cable terminal model with the help of modelling and simulation (Mondal &

Kumbhar, 2016). A series of the common defects, such as scratch of the main insulation, metal particle defects and air gap defects are produced, and the effect on the distribution of the electromagnetic field is studied.

2) Electromagnetic Coupling Mechanism and Propagation Characteristics Analysis

The electromagnetic coupling mechanism in the cable terminal structure is studied based on the transient excitation caused by the partial discharge sources. Electromagnetic field theory states that the discharge caused by the defect is equal to a transient electromagnetic source, which creates rapid electromagnetic disturbances which travel along the cable structure and the adjacent dielectric media.

The propagation behaviour of the electromagnetic signals generated by typical defects is analysed using numerical simulation. The influence of defect geometry, material parameters and structural interfaces on signal attenuation, reflection, superposition and frequency-dependent dispersion properties of electromagnetic wave propagation is discussed. The coupling relationship between the electric field distortion caused by defects and electromagnetic response measurable at remote observation points is studied in particular.

3) Electromagnetic Signal Propagation Analysis and Feature Extraction

The time-domain propagation characteristics of electromagnetic signals generated by cable terminal defects under different operating conditions (such as temperature and humidity) are studied. The numerical simulation method using the finite element method was used to analyse the variation law of electromagnetic signals under different defect types and operating parameters, and representative signal features suitable for defect characterization were extracted (COMSOL AB, 2022).

4) Design and Evaluation of Defect Detection and Diagnosis Methods

Based on the characteristic parameters of different types of cable terminal defects, a detection and diagnosis scheme based on electromagnetic methods was designed using mathematical methods. The diagnostic performance of this scheme was evaluated and compared using indicators such as accuracy, precision, and sensitivity. Finally, an effective method suitable for online detection and diagnosis of cable terminal defects was established.

2. Modelling of 35 kV XLPE cable termination structure and defects

This thesis combines the actual 35kV cable terminal structure and installation process with the selection of Raychem 35kV cable heat shrink outdoor terminal [7]. U Using SolidWorks modelling tools, a 1:1 scale model of an outdoor cable terminal with consistent structure was created.

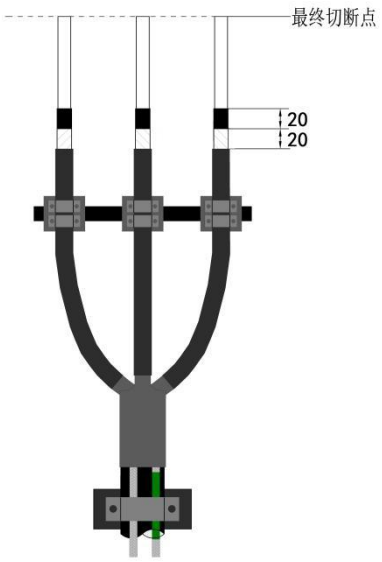

Figure 2-1 Schematic diagram of cable terminal stripping

2.1. 3D geometric modelling of cable terminals

The 3D cross-sectional view of the cable is shown in Figure 2-2 below. The internal and external structure and parameters are as follows: the copper conductor core has a radius of 9.77 mm (conductor cross-sectional area of 300 square meters) and a length of 400 mm. The inner semiconductor layer is 1 mm thick, the main insulation layer is 10 mm thick, the outer semiconductor layer is 1 mm thick, and the bottom copper shielding layer is 0.1 mm thick. The main insulation layer has a scratch located 80 mm axially with a depth of 1 mm. The outer shielding layer covers the entire terminal.

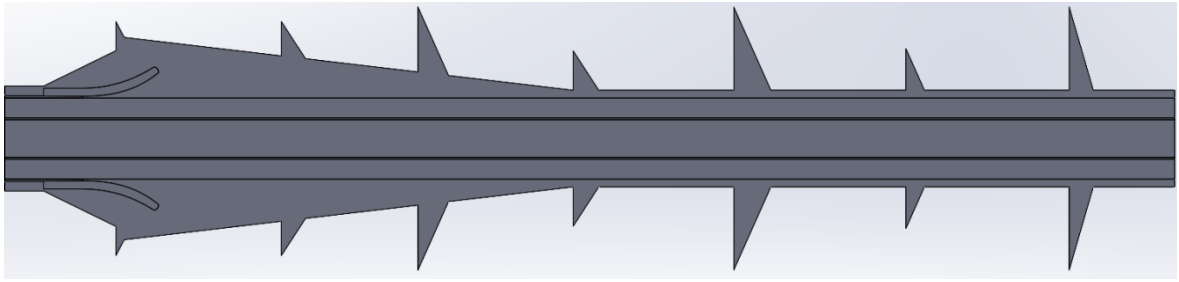

Figure 2-2 Cable terminal cross-section

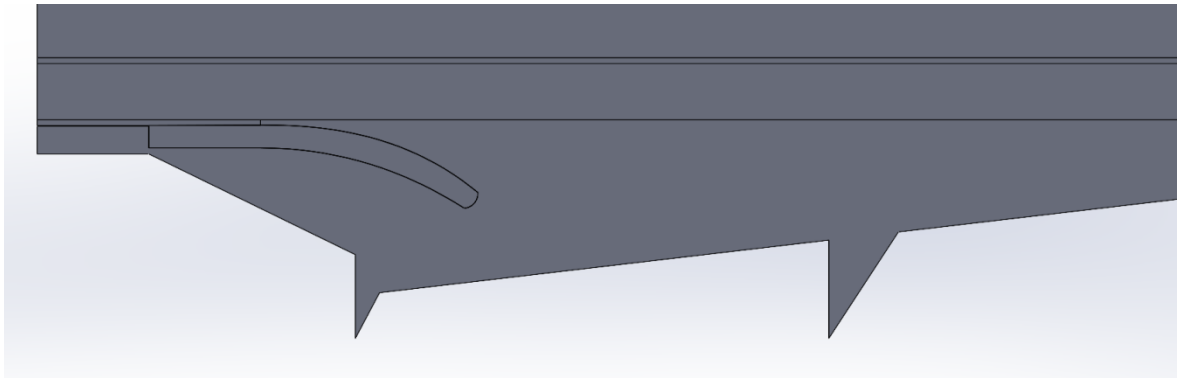

Figure 2-3 Low-voltage end structure and details

This paper simulates three types of cable defects: main insulation scratches, air gap defects, and metal particle defects, and establishes models, as shown in the figure below.

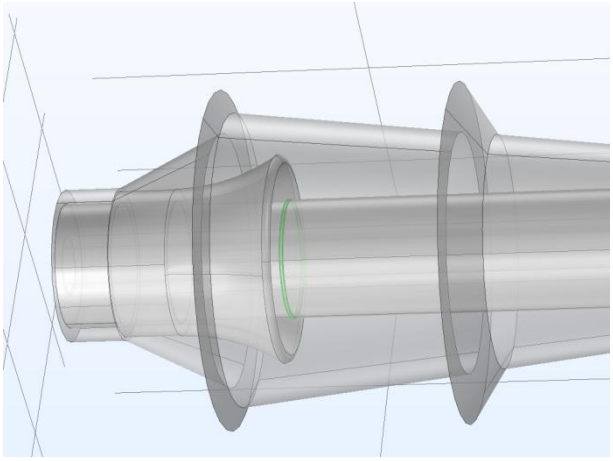

Figure 2-4 Main insulation scratch defects

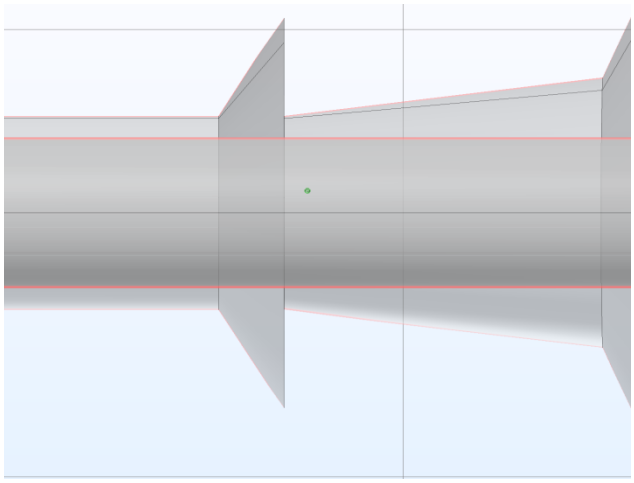

Figure 2-5 Air gap defects

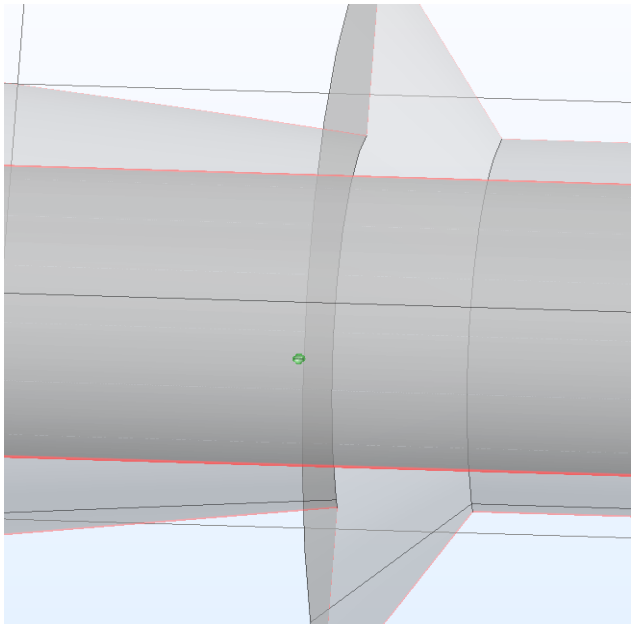

Figure 2-6 Metal particle defects

2.1.2. Simulation parameters and boundary conditions

Based on the actual situation, the relative permittivity and conductivity of each layer of material in the cable termination are shown in Table 2-1. The core and copper shielding layer are made of copper, with a relative permittivity of 1 and a conductivity of 5.998 × 10^7. The relative permittivity of XLPE is 2.35, and its conductivity is 10^-14. The relative permittivity of the external air computational domain is 1, and its conductivity is 0. All other materials have had reasonable parameter settings.

Table 2-1 Cable Termination Structure and Material Properties Table

structure	Relative permittivity	Electrical conductivity (S/m)
Wire core	1	5.998×10^{7}
Inner semiconducting layer	100	10
XLPE	2.35	10^-14
Insulating shielding layer	100	2
Copper shielding	1	5.998×10^{7}
Stress cone	60	1
Terminal main insulation	3	$3e^{-15}$
Air	1	0

2.1.3. Physics field selection and boundary conditions

In electromagnetic field numerical simulations, the electric field distribution is mainly affected by the relative permittivity and conductivity of the dielectric material. Under strictly time-varying electromagnetic field conditions, the electric field distribution is not only related to the permittivity but also influenced by the combined effects of conduction current and displacement current. However, for a 35 kV cross-linked polyethylene (XLPE) cable terminal operating at a power frequency of 50 Hz, its electromagnetic wavelength is much larger than the structural dimensions, and the electric field change process is relatively slow, which can be approximated as a quasi-static process.

Therefore, this paper uses the Electrostatics(es) interface in COMSOL Multiphysics for modelling and analysis. The electrostatic field satisfies the following fundamental governing equations:

$$\nabla \cdot D = \rho_v \tag{2-1}$$

$$E = -\nabla V \tag{2-2}$$

Where ∇ is the vector differential operator, D = ε0εr, ρv is the space charge density, V is the electric potential, and E is the electric field strength.

To simulate the transient electromagnetic disturbances generated when partial discharge occurs in internal defects of cable terminals, this paper does not use the traditional method of applying power frequency voltage to the conductor end, but instead applies an equivalent transient voltage source in the defect region to characterize the electric field excitation effect of the partial discharge source. Therefore, the equivalent excitation signal is represented by a Gaussian pulse function as follows:

$$V(t) = V_0 \exp\left[-\left(\frac{t-t_0}{\tau}\right)^2\right] \tag{2-3}$$

Where V0 is 100kV, representing the equivalent discharge peak amplitude; t0 = 5ns is the pulse centre time; and τ = 1ns is the pulse width parameter.

Copper shield (low-voltage end) grounding, formula as follows:

$$V = 0 \tag{2-4}$$

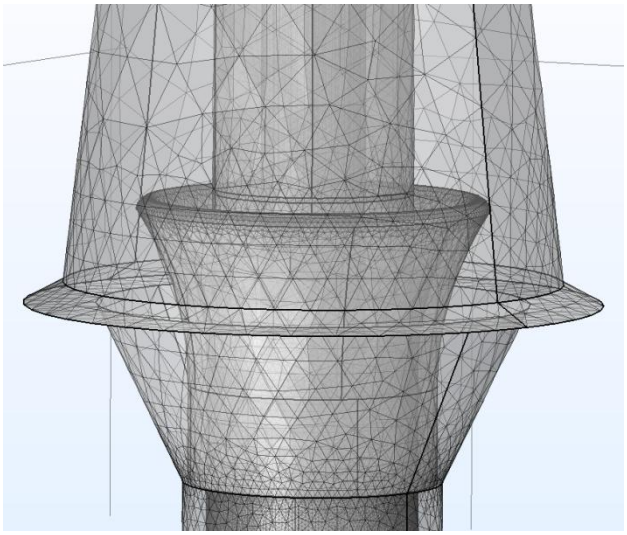

Figure 2-7 Mesh partitioning diagram

The model mesh was generated using COMSOL physical control mesh generation. The system used the finite element method to divide the model into a refined free tetrahedral mesh and perform calculations. To improve the accuracy of electric field calculations in the defect region, local mesh refinement was performed at the defect location. The final mesh consisted of 320,437 tetrahedral elements and 156,114 triangular elements, exhibiting good mesh quality that meets the accuracy requirements for electric field numerical simulation. (See Figure 2-7 for mesh generation diagram.)

3. Comparative Analysis of Transient Electromagnetic Responses under Different Defect Types

Based on the COMSOL model from the previous chapter, pulse voltages were applied to the defects of different defect models, and waveform observation points were added at the low-voltage end of the tail to conduct simulation experiments.

3.1 Main insulation scratch defects

The scratch defect is used to simulate damage to the main insulation layer caused by improper peeling of the insulation shielding layer, and the depth and width of the scratch are set to be similar to those of real scratches. The scratch is located at 81 mm. The scratch is a ring-shaped scratch with a depth of 1 mm, and the cross-section of its electric field simulation result is shown in Figure 3-1.

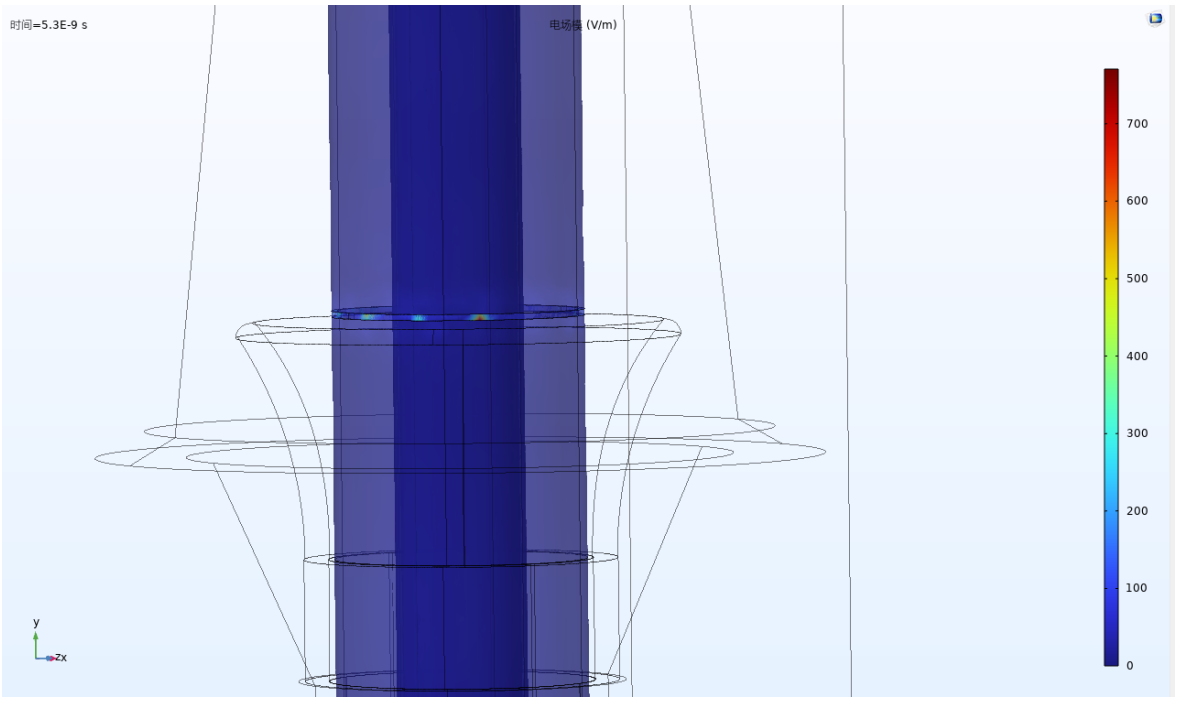

Figure 3-1 Electric field distribution at the scratch at 81 mm

Figure 3-1 shows the spatial distribution of the electric field intensity at the cable termination at $t = 5.3 \times 10^{-9}$ s, which roughly corresponds to the peak value of the applied Gaussian pulse.

It can be seen that the maximum electric field intensity is concentrated in the defect region, shown in red. Meanwhile, a relatively low electric field is distributed in the surrounding main insulation layer, indicating that the transient voltage disturbance generated at the defect is propagating along the cable structure.

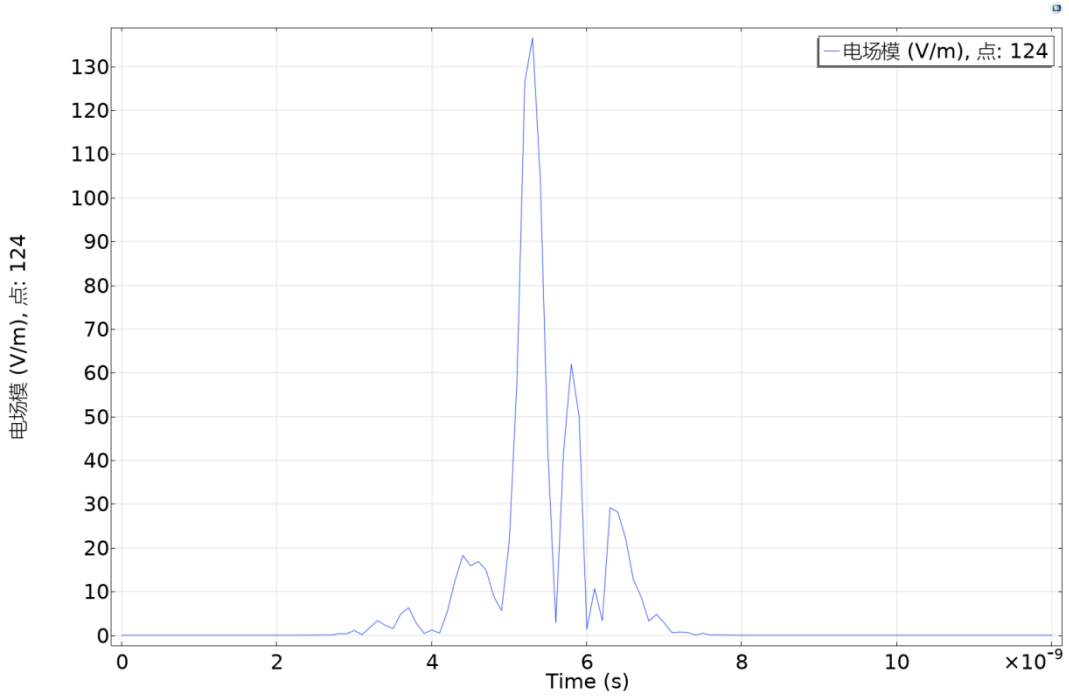

Figure 3-2 Scratch observation point

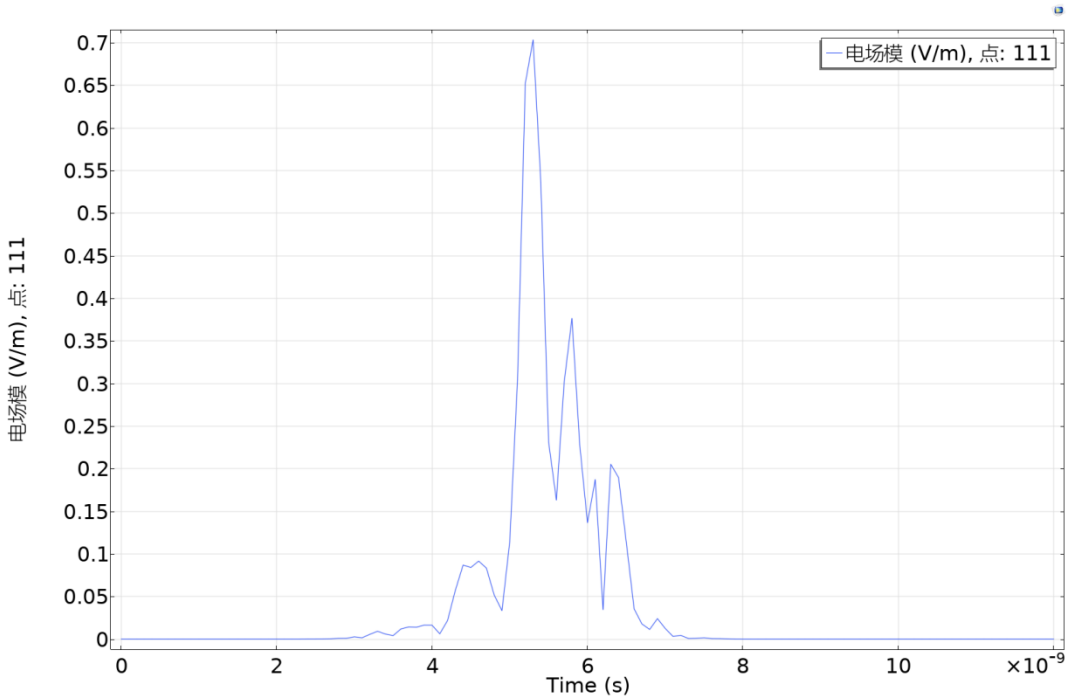

Figure 3-3 Bottom low-pressure end observation point

Figure 3-2 shows in detail the specific time-domain waveform of the electric field at the defect observation point. As can be clearly seen from the graph, the electric field strength increases very quickly within a very small time interval (5.2-5.4×10-9 s) and the rate of change is quite significant, peaking at approximately 135 V/m. This peak is not a coincidence and has a close correlation to the injected Gaussian pulse. Upon careful observation of the waveform, it can be observed that it has a very steep rising edge, indicating that the electric field strength has undergone drastic changes in a very short period of time. Meanwhile, its pulse width is very small and the rise rate is very fast, suggesting that it must be some very important phenomenon, that is, there must be a strong local field enhancement effect at the scratch defect. This effect causes the electric field to exhibit such unique waveform characteristics at the defect location. In addition, after the main pulse, we can also observe a small oscillation phenomenon. After in-depth analysis, it is known that this phenomenon is mainly caused by the reflection and superposition of electromagnetic waves at material interfaces (such as interfaces between insulation layers, semiconductor layers, and stress cones of different types). These complex physical processes collectively lead to small oscillations after the main pulse.

Figure 3-3 focuses on the waveform situation at the low voltage end. When we compare the waveform at the low voltage end with the waveform at the defect location, a significant difference immediately becomes apparent, which is the significant change in peak intensity. At the low voltage end, the peak intensity significantly decreases, only about 0.7V/m, and the attenuation rate is close to 99% compared to the 135 V/m at the defect site. This significant attenuation clearly indicates the existence of significant energy loss during the propagation of the electric field. However, interestingly, despite the huge difference in peak intensity, the peak arrival times of the two points are almost the same. This phenomenon can be attributed to the characteristics of XLPE (cross-linked polyethylene) material. In XLPE, due to the relatively short propagation distance and high wave velocity, the time delay is very small, making it difficult to distinguish the time difference between the two in actual measurements.

3.2 Air gap defects

Air gap defects are usually caused by incomplete insulation filling, improper installation of stress control components, or insufficient interlayer bonding of materials, which may result in trace gas retention. Since the relative permittivity of air ($\varepsilon r \approx 1$) is much lower than that of XLPE insulation ($\varepsilon r \approx 2.3$), air gaps distort the local electric field and increase its intensity nearby.

In this study, the air gap defect is simplified as a 1 mm diameter spherical inclusion located 313.69 mm from the bottom observation point within the main insulation layer. Based on this model, the transient electric field response under pulse excitation is analysed.

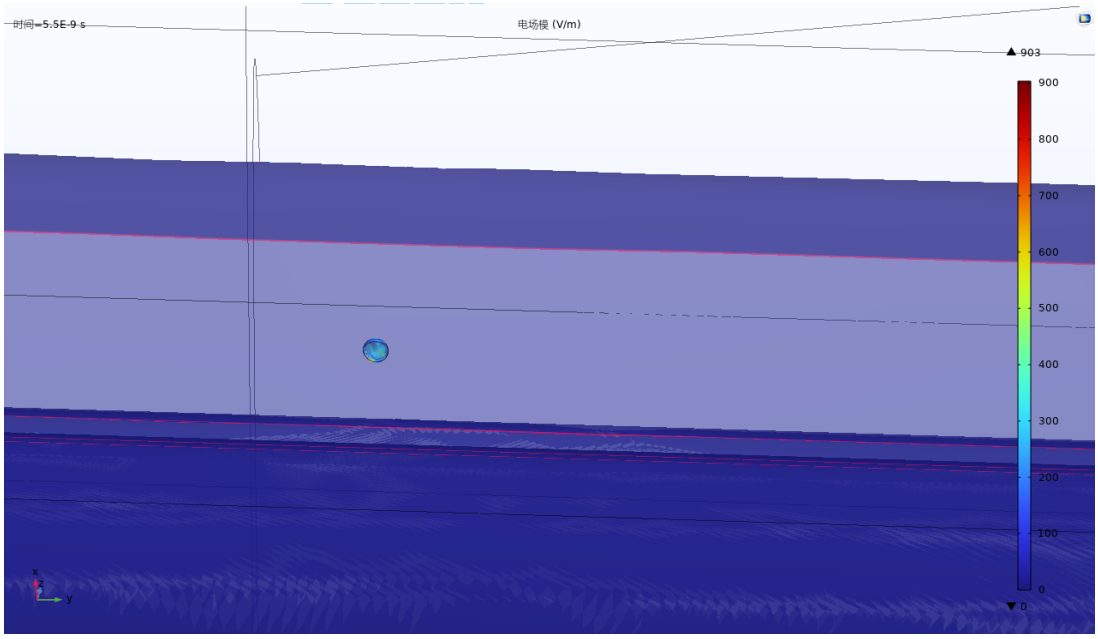

Figure 3-4 Electric field diagram of an air gap defect with a diameter of 1 mm

It can be observed that the electric field is significantly intensified inside the void region. The maximum electric field intensity (red area) appears at the local boundary of the air gap, rather than being uniformly distributed within the air gap or surrounding insulation layer.

Although most of the insulation region is blue in the contour plot, indicating relatively low intensity, a weak electric field still exists. This shows that the transient electromagnetic disturbance is not limited to the defect, but spreads into the adjacent main insulation layer.

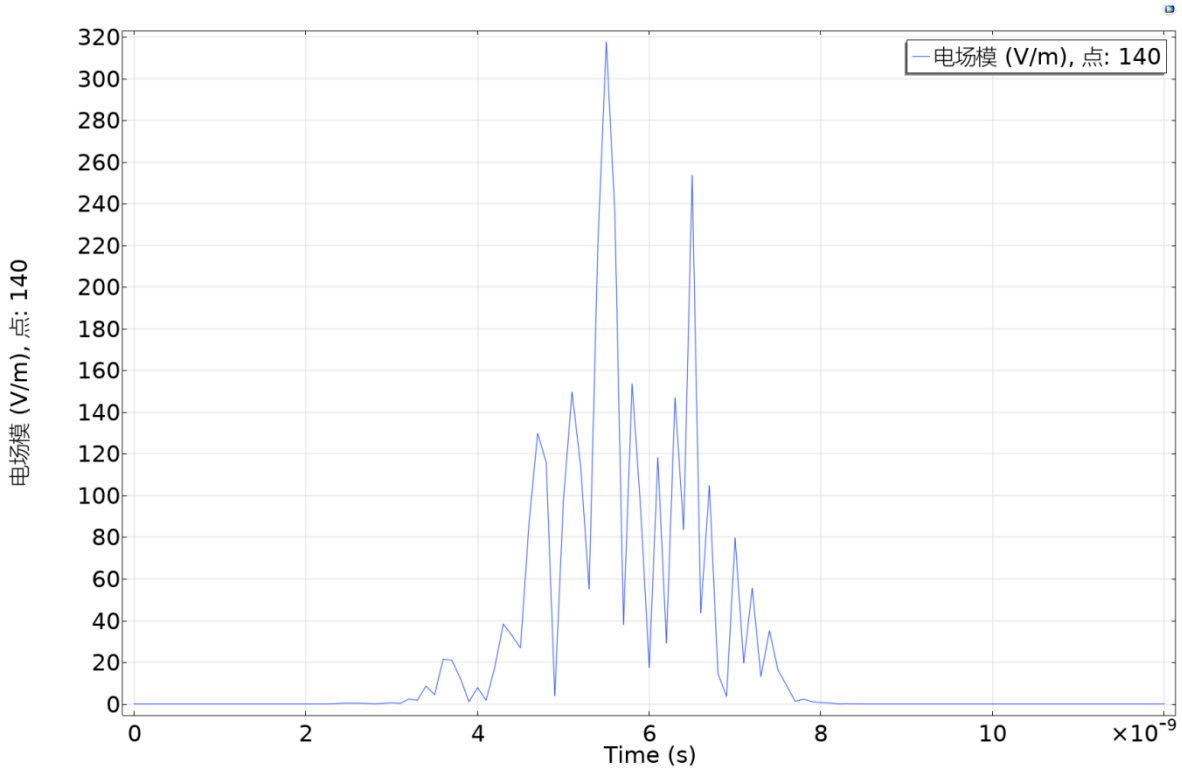

Figure 3-5 Air gar observation point

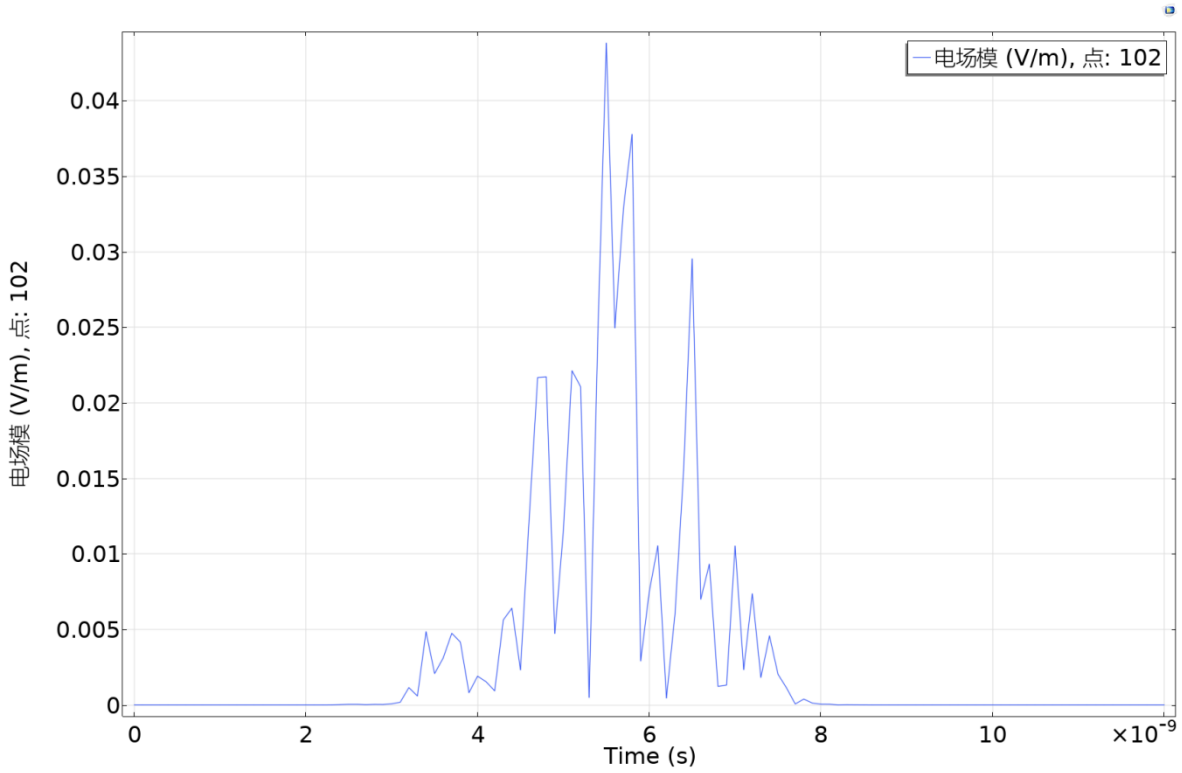

Figure 3-6 Bottom low-pressure end observation point

The time-domain waveform of the electric field at the air gap defect is shown in Figure 3-5. A significant main peak appears at 5.5 ns, with a peak value of approximately 315 V/m. The rising edge is steep and the main pulse width is narrow, indicating that there is a significant local field enhancement effect in the air gap region. The circular geometry of the air gap can also lead to an increase in the number of oscillation peaks. Due to its closed and curved interface, multiple internal reflections and local resonance effects occur, resulting in richer high frequency components in the transient response. In addition, multiple oscillating peaks appear after the main peak, indicating that the air gap interface causes multiple reflections and superpositions, resulting in a rich high-frequency component.

At the bottom observation point, the greatest electric field is greatly reduced to about 0.043 V/m, as illustrated in figure 3-6. This is almost 99.98% of the energy being lost from the transient electromagnetic wave during its travel through the cable terminus, which is far greater than the loss of energy through the defect region (315 V/m). In addition, the waveform received 6.5 ns later at the far end is smoother than at the source region, exhibiting good attenuation and filtering features, with the main peak having broadened and reduced in amplitude.

3.3 Metal particle defects

Research papers and related materials reveal that copper particles are the most common type of metal particle defect in modern cable terminals. These conductive impurities that cause defects are usually located near the main insulation layer. They may be due to copper shavings generated during conductor cutting and crimping, or copper detachment caused by poor terminal crimping, appearing as flakes or spheres.

The corresponding electric field distribution is presented in Figure 3-7. In this case, only the material parameter is varied as a control condition.

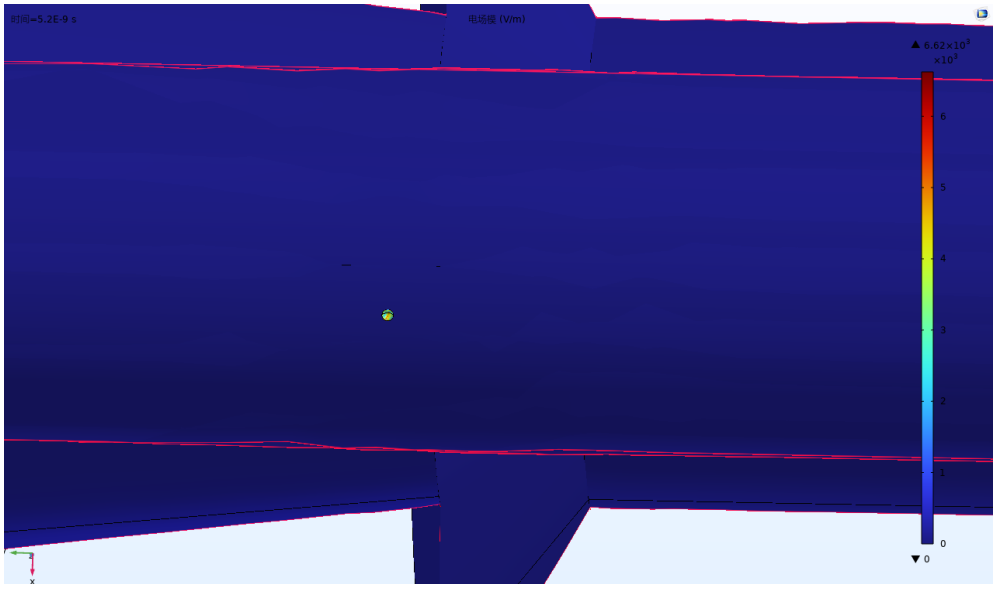

Figure 3-7 Electric field diagram of metal particle defects

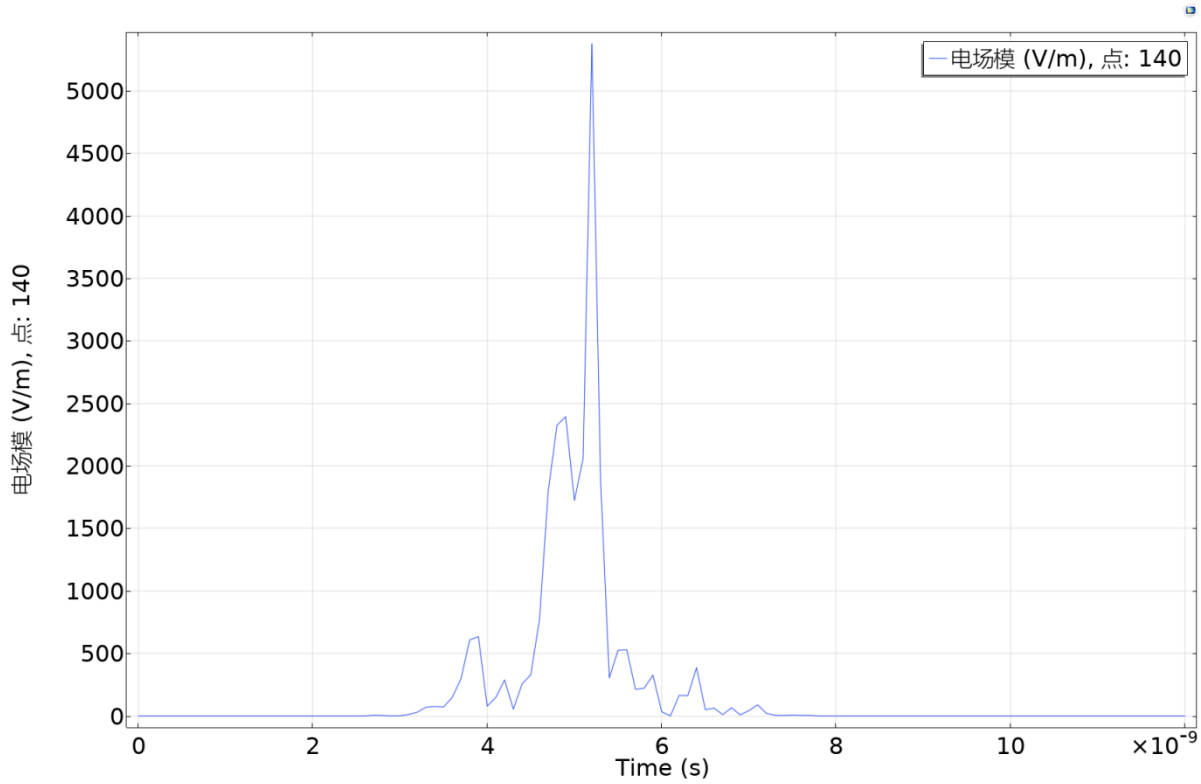

Figure 3-8 Metal particle observation point

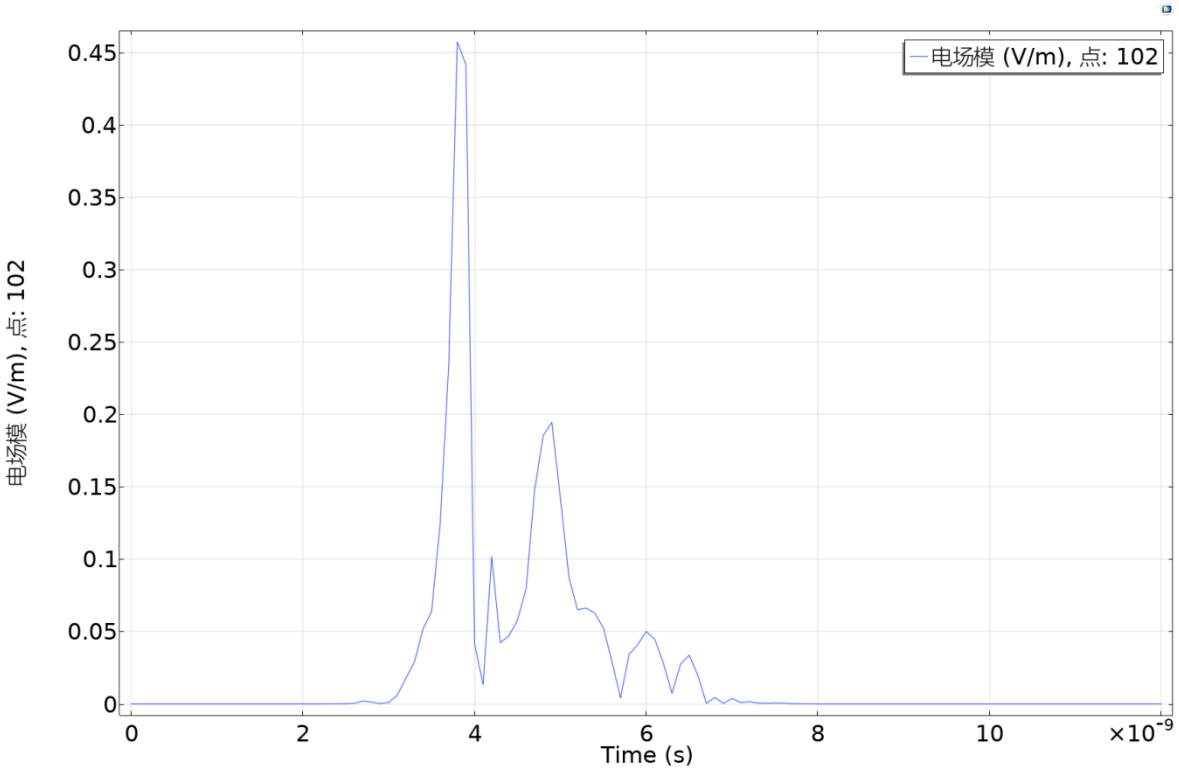

Figure 3-9 Bottom low-pressure end observation point

As shown in Figure 3-8, the main peak of the wave appears at approximately 5.0–5.2 ns, with a peak value of approximately 5200 V/m and an extremely steep rise. This is because copper has extremely high conductivity ($\sigma \approx 5.8*10^7$ S/m), forming an equipotential body on its surface under the influence of an electric field, with charges accumulating at the tips. In addition, the small radius of curvature also contributes to the high electric field strength.

At the bottom observation point, gradually increasing small peaks can be observed in the 3.5–4.5 ns range. These early weak oscillations are probably related to the arrival of transient wavefront and the superposition of reflection components at the material interface. The peak value is about 0.45 V/m, and the attenuation rate is 99.991%. The main peak is followed by a significant oscillation, accompanied by multiple secondary peaks.

4. Signal Propagation Characteristics Extraction and Mathematical Analysis under Typical Defect Conditions

4.1 Time-Domain Feature Extraction

The following representative time-domain features were extracted from the transient electric field waveforms to quantitatively analyse the differences between different defects.

(1) Peak Electric Field:

$$E_{max} = \max(|E(t)|) \tag{4-1}$$

(2) Pulse width:

$$FWHM = t2 - t1 \tag{4-2}$$

The intensity of this transient event is indicated by the pulse width.

(3) Signal Energy:

$$W = \sum_{i=1}^{N} E_i^2 \Delta t \tag{4-3}$$

(4) Attenuation ratio:

$$\eta = \frac{E_{bottom,max}}{E_{defect,max}} \tag{4-4}$$

All these parameters are used to globally represent the characteristics observed in the waveform, allowing for identification and classification of the defects type in subsequent stages.

4.2 Frequency-Domain Characteristic Analysis

The mathematical technique of Fast Fourier Transform (FFT) was used to further analyse the spectral characteristic of various defects (Marks, 2009). The dominant frequency and spectral bandwidth are extracted to evaluate high-frequency components:

$$F(f) = \sum_{n=0}^{N-1} E(n) e^{-j2\pi fn/\mathrm{N}} \tag{4-5}$$

4.3 Quantitative Comparison of Different Defects

Table 4-1 Eigenvalue table

Defect	Peak (V/m)	Bottom Peak (V/m)	Pulse width (ns)	Attenuation η	Oscillation	Signal Energy	Dominant Frequency (GHz)
Scratch	135	0.7	0.6	5.2×10^{-3}	4	2.94×10^{-10}	1.0
Air Gap	315	0.043	0.4	1.4×10^{-4}	5	7.4×10^{-13}	2.0
Metal particle	5200	0.47	0.2	8.6×10^{-5}	8	4.05×10^{-11}	3.0

In the figure above, metal particle defects exhibit the highest peak electric field and the richest high-frequency components, whereas scratch defects exhibit a relatively mild enhancement in the electric field and a wider pulse width. These quantitative differences provide a reliable basis for defect classification.

4.4 Defect Classification Based on Support Vector Machine

In the preceding text, characteristic parameters of typical defects were extracted from the time and frequency domains. To achieve intelligent identification of cable terminal defect types, this paper employs the Support Vector Machine (SVM) algorithm to construct a multi-classification identification model.

4.4.1 Feature Vector Construction

Based on the statistical results in Table 4-1, six characteristic parameters were selected to construct the sample feature vector: peak electric field at the low voltage end (bottom), pulse width (tw), signal energy (W), attenuation coefficient (η), oscillation number (Nosc), and dominant frequency (fd).

Compared to the peak electric field parameters at the defect (which cannot be directly located and measured), the low-voltage end observations are more in line with actual

online detection conditions. Therefore, this paper selects remotely measurable features as classification input variables to improve the engineering feasibility of the method.
Constructing a six-dimensional eigenvector:

$$X = [E_{bottom}, t_w, W, \eta, N_{osc}, f_d] \tag{4-6}$$

4.4.2 Sample expansion and data preprocessing

Due to the limited number of simulation samples, multiple simulations and random perturbations were used to expand the sample size to improve model stability and generalization ability. Based on the original characteristic values of various defects, Gaussian random perturbations within a 30% amplitude range were introduced:

$$X_i^{new} = X_i \cdot (1 + 0.3 \cdot randn) \tag{4-7}$$

200 samples are generated for each type of defect, resulting in a total of 600 training samples.
To eliminate the influence of differences in the dimensions of different features, the Z-score standardization method is used for data normalization:

$$X' = \frac{X-\mu}{\sigma} \tag{4-8}$$

Where μ is the sample mean and σ is the standard deviation.
Since the defect category is a three-class classification problem, this paper adopts the Error Corrected Output Encoding (ECOC) strategy to construct a multi-class support vector machine model. The kernel function is selected from radial basis functions (RBF):

$$XK(x_i, x_j) = \exp(-\gamma|x_i - x_j|^2)' \tag{4-9}$$

This kernel function can effectively handle nonlinear separable problems.
To avoid overfitting, this paper employs 5-fold cross-validation to evaluate model performance. The cross-validation accuracy is calculated using the following formula:

$$X = \text{Accuracy} = 1 - \text{Loss} \tag{4-10}$$

This formula can be used to make a preliminary assessment of the model's accuracy.

4.5 Model accuracy analysis and result evaluation

The confusion matrix is shown in the figure 4-1 based on the cross-validation results. A total of 600 samples participated in the validation, of which 598 samples were correctly classified and only 2 samples were misclassified.

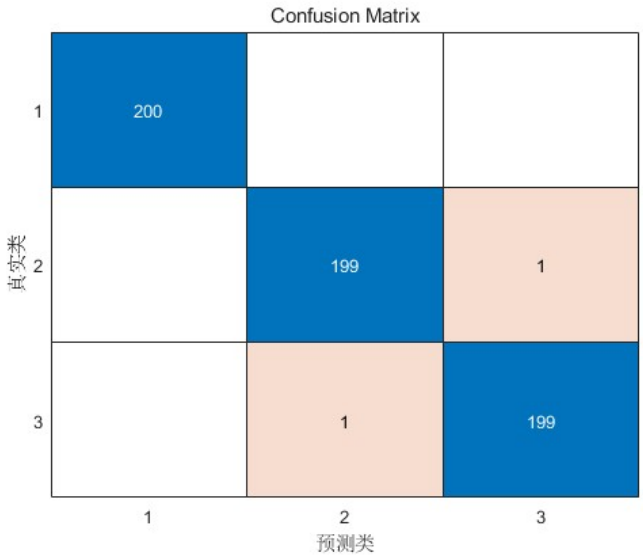

Figure 4-1 Confusion Matrix of SVM-Based Cable Terminal Defect Classification

The overall classification accuracy rate is:

$$Accuracy = \frac{598}{600} = 99.67\% \tag{4-11}$$

The results show that the constructed SVM model has extremely high classification accuracy and can effectively distinguish three typical defects.

Table 4-2 Precision and recall rates for each defect category

Defect	Precision	Recall
Scratch	100%	100%
Air Gap	99.5%	99.5%
Metal particle	99.5%	99.5%

The confusion matrix shows that misjudgements only occurred between air gap defects and metal particle defects, and there was no confusion with scratch defects.

The reason for a small number of misjudgements may be that, during the expansion of random perturbation samples, the dominant frequency or oscillation number of some air gap and metal particle samples may locally overlap. Both of these defects exhibit strong high-frequency components and narrow pulse widths, resulting in local intersections at the feature space boundaries during computation. Alternatively, when the set perturbation amplitude is

large (30%), some samples may deviate from the original physical feature range, leading to numerical domain overlap.

However, overall, the misjudgement rate was only:

$$Error = \frac{2}{600} = 0.33\% \tag{4-12}$$

This demonstrates that the model is highly robust.

Furthermore, the classification results show that scratch defects are clearly distinguishable from the other two types in the feature space. Compared with air gap and metal particle defects, scratch defects have lower peak electric field intensity, wider pulse width, and weaker high-frequency components. The support vector machine (SVM) classifier has some unique advantages and characteristics that make it perform particularly well in handling classification tasks. Especially in scenarios where it is necessary to distinguish between two different things, SVM can generate a very clear and distinct boundary line, thereby achieving accurate recognition results. When we apply it to the classification task of air gap defects and metal particle defects, we can observe from Figure 4-1 that although these two types of defects may exhibit certain overlapping areas in some cases, their overall discriminability is still high. After in-depth analysis of the waveform diagrams corresponding to these two types of defects, it can be further discovered that both air gap defects and metal particle defects can cause a strong and instantaneous electromagnetic interference phenomenon. The characteristic of this interference is its extremely short duration, accompanied by a large number of high-frequency components, which may cause two types of defects to exhibit similar characteristics under specific conditions, occasionally leading to classification errors. However, the probability of this situation occurring is very low, only about 0.05%, so the impact on overall classification performance is minimal.

In order to further improve the classification accuracy of the model and enhance its robustness, we adopted a five fold cross validation method in our research. The concept of this approach is to split the data into five sub-sets and alternate between using four of them as training data and the remaining one as testing data, and then comprehensively analyse all the test results. This method can not only be used to have a comprehensive analysis of the performance of the model under various data partition conditions, but also can effectively prevent overfitting of the training data and bring insufficient generalization ability to the model. This is because this technique significantly decreases the chance of the model learning the training data by heart and not generalizing it to new and unseen data.

Our proposed method using feature extraction and support vector machine (SVM) classifier has proved to be very good overall. This technique is fairly good as far as stability and adaptability to new situations. Despite the complex and dynamic application scenarios in practice, it can still achieve good classification accuracy, truly showing its value and engineering application potential.

5. Conclusions

The article expounds the electromagnetic properties of common defects of 35kV cross-linked polyethylene (XLPE) cable terminal and analyzes the intelligent identification methods of these defects. The inherent relationship between various defects and electromagnetic signals was scientifically studied by combining electromagnetic field simulation technology with machine learning classification algorithms, which not only laid the foundation for the theoretical analysis of the electromagnetic signals generated by various types of defects in the cable terminal, but also provided technical support for the accurate detection of cable terminal defects. The following is a summary of the main research results and conclusions.

To simulate the actual working conditions as close as possible, this study created a high accuracy 3D simulation model of the 35KV XLPE cable terminal using two software (SolidWorks and COMSOL Multiphysics). This model is created from the structural parameters of actual cables, taking into account the important factors, including geometric shape, material properties, boundary conditions, etc. On this basis, detailed modeling work was carried out for three typical installation defects - scratches on the main insulation layer, air gap defects, and metal particle contamination. By accurately describing the morphology and distribution of these defects, the reliability and authenticity of the simulation results are ensured. Under equivalent Gaussian pulse excitation conditions, the transient electromagnetic response characteristics excited by the above-mentioned defects were further analyzed, revealing the influence of different defects on electromagnetic signals and their unique characteristics. The simulation results show that different defects produce significantly different electric field distributions and transient electromagnetic signals.

Then, the transient electromagnetic characteristics of different defect types were analysed in the time domain. The results show that, due to the strong electric field concentration effect caused by conductive particles, among the three typical defects, the peak electric field intensity produced by metal microparticle defects is the highest (5200 V/m), followed by air gap defects (315 V/m), and scratch defects (135 V/m) are the lowest. Furthermore, their waveform characteristics, such as pulse width, oscillation number, dominant frequency, and attenuation characteristics, show significant differences. These characteristics effectively

describe the amplitude, time characteristics, energy distribution, and spectral characteristics of the transient electromagnetic signal. Quantitative comparisons show that the extracted features can relatively clearly distinguish different defect types.

This article uses Support Vector Machine (SVM) as the basic algorithm to construct a model specifically for defect classification. In practical operation, specific classification problems are solved by extracting relevant feature parameters. In the construction phase of the model, in order to effectively address the challenging problem of nonlinear classification, the ECOC (Error Correction Output Code) multi classification strategy was specifically adopted, combined with radial basis function kernel functions for processing. At the same time, in order to increase the diversity of data and the robustness of the model, data augmentation operations are performed by adding perturbation samples to the original data. In addition, Z-score normalization was applied to the data, and after this series of operations, a model with a sample size of approximately 600 was finally obtained, which greatly improved the reliability of the modeling. In order to comprehensively evaluate the performance of the model, a five fold cross validation method was used to test it. The test results show that the overall classification accuracy is as high as 99.67%. Specifically, the recognition rates for three different types of defects, namely scratch defects, air gap defects, and metal particle defects, reached 100%, 99.5%, and 99.5%, respectively. These data fully demonstrate that the model has a very strong classification ability in defect recognition, which can effectively distinguish different types of defects.

To sum up, it has been a multi-faceted study from modeling based on actual model size to simulation analysis to waveform classification to verification which has brought a lot of results. Not only have these achievements important application engineering value, but also have extraordinary significance in academic circles, which have provided solid theoretical support for the diagnosis and development of online monitoring technology for cable terminal faults, and are expected to make positive contributions to related disciplines.

5.1 Future Work Outlook

If we take a comprehensive look at the existing research status and practical engineering requirements, it can be seen that there are still several aspects that need to be improved and

optimized in order to comprehensively grasp the scientific value of the existing research.In view of the overall status of research and practical engineering requirements, some progress has been made in defect modeling, electromagnetic signal analysis and intelligent classification technology, and relatively accurate mathematical models have been developed, but it is not difficult to see that there are still a number of aspects that need to be further improved and optimized.

The research in this article is mainly based on numerical simulations under ideal conditions. In practical applications, however, environmental noise, sensor nature and measurement errors are also all important to the acquisition and interpretation of electromagnetic signals, and cannot be ignored. In this case, it is better to use a real cable terminal testing platform for the verification as far as possible when conditions are favorable. Theories are analyzed and verified with experiments, and more reliable and convincing research results can be gathered.

As far as the physical model is concerned, the current 3D model is actually the defect morphology under idealized conditions. Defects in practical applications can be very complex, with irregular gaps, metal fragments, interactions between multiple defects or aging effects due to prolonged use. Future research is needed in the development of models more aligned to practical application scenarios, and in a more detailed study of the effect of defect size, location, and combinations of size and location on the characteristics of the signal.

In terms of algorithms, currently only support vector machines (SVM) are used for classification tasks. Although KNN (K-nearest neighbor algorithm) and decision trees perform quite well in similar scenarios, they have not yet been compared and studied. With the continuous advancement of artificial intelligence technology, methods such as artificial neural networks (ANN), convolutional neural networks (CNN), and ensemble learning are expected to further improve the accuracy and robustness of classification. Thus, it is important to increase the scope of the actual measurement samples and to actively use these sophisticated algorithms to enhance research work.

The classification and recognition function of defects are the main functions of the model proposed in this article. In practical applications, based on defect localization, various functions such as early warning, classification, and localization can be implemented in the future, which will significantly increase its application value in the engineering field if it can

be effectively combined with real-time monitoring. This can contribute to enhancing the safety and reliability of equipment operation, and also serve as a reference and inspiration for research and development in related fields.

References

COMSOL AB. (2022). COMSOL Multiphysics Reference Man.

Corporate Author Name. (n.d.). 35 kV cable accessory installation technical manual.

Govindarajan, S., Morales, A., Ardila-Rey, J. A., & Purushothaman, N. (2023). A review on partial discharge diagnosis in cables: Theory, techniques, and trends. Measurement, 216, 112882. https://doi.org/10.1016/j.measurement.2023.112882

G. C. Stone. (2005). Partial discharge diagnostics and electrical equipment insulation condition assessment. IEEE Transactions on Dielectrics and Electrical Insulation, 12(5), 891–904. https://doi.org/10.1109/TDEI.2005.1522184

Huang, T. (2022). Research on power-frequency partial discharge characteristics of typical installation defects of 10 kV cable terminals (Master's thesis). South China University of Technology.

Illias, H. A., Lee, Z., Bakar, A., et al. (2012). Electric field distribution in 132 kV one piece premolded cable joint structures. 2012 IEEE International Conference on Condition Monitoring and Diagnosis, 643–646.

Kaziz, S., et al. (2023). Radiometric Partial Discharge Detection: A Review. Energies.

K. Yamashita, T. Miyake, T. Sakoda & W. Kawano. (2019). Study on Location Accuracy of Partial Discharge Locator. 2019 IEEE Electrical Insulation Conference (EIC), Calgary, AB, Canada, 321–324. https://doi.org/10.1109/EIC43217.2019.9046611

Li, H. M. (2022). Research on electric field distribution and structure optimization of 220 kV cable terminal under dynamic parameters (Master's thesis). Harbin University of Science and Technology.

LI Ming, Fredrik Sahlen, Stefen Halen, et al. (2004). Impacts of high-frequency voltage on cable termination with resistive stress grading. International Conference on Solid Dielectrics, Vasteras, Sweden, 300–303.

Liu, G., & Chen, Z. (2012). Experiment of main insulation with air gap of 10 kV cross-linked polyethylene cable terminal. High Voltage Engineering, 38(3), 678–683. https://doi.org/10.3969/j.issn.1003-6520.2012.03.023

L. Niemeyer. (1995). A generalized approach to partial discharge modelling. IEEE Transactions on Dielectrics and Electrical Insulation, 2(4), 510–528. https://doi.org/10.1109/94.407017

Marks, R. J. (2009). Handbook of Fourier Analysis & Its Applications.

Mondal, M., & Kumbhar, G. B. (2016). Partial discharge localization in a power transformer: methods, trends and future research. IETE Technical Review.

Morshuis, P. H. F. (2005). Degradation of solid dielectrics due to internal partial discharge: some thoughts on progress made and where to go now. IEEE Transactions on Dielectrics and Electrical Insulation, 12(5), 905–913.

Shafiq, M., et al. (2019). Online condition monitoring of MV cable feeders using Rogowski coil sensors.

Sheng, B., Lewin, P. L., et al. (2014). Partial discharge pulse propagation in power cable and attenuation in monitoring systems. IEEE Transactions on Dielectrics and Electrical Insulation.

Tanaka, T. (2005). Dielectric nanocomposites with insulating properties. IEEE Transactions on Dielectrics and Electrical Insulation, 12(5), 914–928.

Y. Hongquan et al. (2022). Application of UHF and HFCT Partial Discharge Detection in GIS Cable Terminal Defect. 2022 IEEE International Conference on High Voltage Engineering and Applications (ICHVE), Chongqing, China, 1–5. https://doi.org/10.1109/ICHVE53725.2022.10014507